

Thick and old sea ice in the Beaufort Sea during summer 2020/21 was associated with enhanced transport

G.W.K. Moore ^{1,2}, Michael Steele³, Axel J. Schweiger ³, Jinlun Zhang³ & Kristin L. Laidre³

The Arctic Ocean has seen a remarkable reduction in sea ice coverage, thickness and age since the 1980s. These changes are most pronounced in the Beaufort Sea, with a transition around 2007 from a regime dominated by multi-year sea ice to one with large expanses of open water during the summer. Using satellite-based observations of sea ice, an atmospheric reanalysis and a coupled ice-ocean model, we show that during the summers of 2020 and 2021, the Beaufort Sea hosted anomalously large concentrations of thick and old ice. We show that ice advection contributed to these anomalies, with 2020 dominated by eastward transport from the Chukchi Sea, and 2021 dominated by transport from the Last Ice Area to the north of Canada and Greenland. Since 2007, cool season (fall, winter, and spring) ice volume transport into the Beaufort Sea accounts for ~45% of the variability in early summer ice volume—a threefold increase from that associated with conditions prior to 2007. This variability is likely to impact marine infrastructure and ecosystems.

¹Department of Physics, University of Toronto, Ontario, ON, Canada. ²Department of Chemical and Physical Sciences, University of Toronto Mississauga, Mississauga, ON, Canada. ³Polar Science Center, Applied Physics Laboratory, University of Washington, Seattle, WA, USA. ✉email: gwk.moore@utoronto.ca

July and August 2020 saw unprecedented low sea ice concentration in the Wandel Sea to the north of Greenland, a region that is normally characterized by a thick and compact multi-year ice cover¹. The Wandel Sea is the eastern part of the Last Ice Area (hereafter, LIA, the area north of Greenland and the Canadian Arctic Archipelago), where thick multi-year ice is predicted to last longer than other regions in the Arctic and is expected to provide a refuge for ice-dependent species^{2–4}. It has been argued¹ that the summer 2020 Wandel sea ice minimum was caused by a long-term trend towards a thinner ice pack as well as anomalous atmospheric circulation during the summer that advected ice out of the region. Interestingly, winds during the preceding winter had also advected thick and old ice into the region, but this was found to have minimal effect on end-of-summer conditions.

At the same time the Beaufort Sea, located over 2100 km to the southwest of the Wandel Sea, had sea ice that was 50% higher in area-mean average concentration, 3 years older, and up to 1 m thicker than climatological means over 2007–2019 (Fig. 1). Please see Section 2 for a rationale for this choice of a climatological period. A similar situation also occurred during the summer of 2021 (Fig. 1), which was characterized by the largest pan-Arctic September sea ice extent since 2014⁵.

There is evidence⁶ that the Beaufort Sea underwent a transition around 2007 from a state dominated by thick multi-year ice to one with a more seasonal ice cover. In general, a reduction in multi-year ice may result in a transient benefit to some ecosystems because of an increase in primary and secondary productivity with thinner ice that can be more easily penetrated by solar radiation^{7–11}. In some areas this may confer temporary benefits to ice-dependent species that rely on springtime production for foraging¹². However, high interannual variability in sea ice characteristics, together with increased sea ice mobility, can also lead to unfavorable conditions for species that require sea ice at specific times of the year for survival and reproduction^{13–15}.

The distribution of Arctic sea ice is, to leading order, controlled by the surface wind field¹⁶ with the Beaufort High, a quasi-permanent high pressure center associated with anticyclonic winds¹⁷, playing a leading role. These winds drive anticyclonic ice motion which in turn produces Ekman convergence in the upper ocean. The resulting concentration of relatively fresh surface water in the region leads to higher sea levels and anticyclonic geostrophic ocean currents. The anticyclonic ice and ocean currents are collectively referred to as the Beaufort Gyre¹⁸. Here we focus on two aspects of the climatological sea ice anticyclone: the import of ice into the Beaufort Sea from the north (especially from the LIA), and the export of ice from the Beaufort Sea to the west into the Chukchi Sea. The latter is generally larger than the former¹⁹.

It has been noted²⁰ that low sea ice conditions in the Beaufort Sea during the summer of 1998 were, during the preceding cool season, associated with low sea-level pressures over the western Arctic that contributed to a reduction of thick ice import from the north into the Beaufort Gyre. They proposed that this resulted in a thinner ice pack in the Beaufort Sea that was easier to melt out during the following summer. Alternatively, it has been argued²¹ that an enhanced westward sea ice export to the Chukchi Sea during January–April 2016 contributed to ice-free Beaufort Sea conditions during September 2016, which was shown to be associated with a strengthened Beaufort High.

More recently, the May 2020 development of a polynya north of Ellesmere Island²², the July–August 2020 Wandel Sea ice minimum¹, and the December 2020 through February 2021 anomalous ice transport into the Beaufort Sea from the LIA²³ were all associated with enhanced anticyclonic winds that were the result of a strengthened and expanded Beaufort High with a center further north and east than in the climatology. On the

other hand, some recent winters (hereafter defined as January, February, and March) have seen a collapse of the Beaufort High, resulting in a reversal of winds from anticyclonic to cyclonic²⁴. In particular, the reversal that occurred during winter 2017 resulted in a corresponding reversal of the Beaufort Gyre sea ice motion, with ice convergence into the eastern Beaufort Sea²⁴ and a thicker ice pack²⁵. The Beaufort High also collapsed during winter 2020²⁶.

In this paper, we investigate the processes that resulted in the presence of anomalously large amounts of thick and old sea ice in the Beaufort Sea during the summers of 2020 and 2021. We seek to understand the similarities and differences in the forcing that resulted in these anomalous conditions as well as more broadly assessing the role of cool-season advection on summer ice conditions. We use a variety of data sources for our analysis, including those derived from satellites, reanalysis, and numerical models (see Methods section).

Results

Identification of a regime shift in Beaufort summer sea ice characteristics. Figure 2 shows time series of Beaufort Sea summer sea ice concentration, sea ice age, and sea ice thickness, as well as the ratio of Beaufort ice volume to that of the entire Arctic²⁷. We define the summer to be the months of July, August, and September. A step function has been fit to the time series with a breakpoint determined by a minimization of the root-mean square fit to the data with a significance test of the difference of the means that takes into account the temporal autocorrelation of geophysical time series²⁸; see Methods Section for further information. The first three metrics (Fig. 2a–c) indicate a transition toward less extensive, thinner and younger ice pack occurred around 2007. Furthermore, the Beaufort's contribution to total Arctic ice volume decreased in 2007 from approximately 10% to 5% (Fig. 2d). We will refer in this study to the period from 2007–present as the “young ice regime,” while the period prior to 2007 will be referred to as the “old ice regime.” All metrics indicate that the summers of 2020 and 2021 (as well as 2013), stand out with ice characteristics above the mean for this new ice regime. This is especially true for the ice volume ratio where values for these past two summers approach those typical of conditions prior to the 2007 transition.

Sea ice conditions during 2019/2020 and 2020/2021. Figure 3 shows time series of Beaufort Sea ice concentration and thickness for the 2-year period October 2019–September 2021, as well as climatological values for the first 13 years of the young ice regime (2007–2019) and anomalies with respect to these 13 years. The results show that starting in May of both years, concentration and thickness were both higher than the climatology by at least 1 standard deviation. The area-mean thickness anomaly was larger in 2020, while the sea ice concentration anomaly was larger in 2021.

Figure 4 provides the Beaufort Sea ice thickness and age distributions in summer for (i) the first 13 years of the old ice regime (1979–1991) when the region was dominated by multi-year ice, (ii) the first 13 years of the young ice regime (2007–2019), (iii) the year 2020, and (iv) the year 2021. A kernel smoothing technique²⁹ was used to fit the distributions to the data. The old ice regime was dominated by thick, old ice, with smaller contributions from thin, young ice. In contrast, the young ice regime is dominated by thin, young ice with a long “tail” of thick, old ice. The years 2020 and 2021 are representative of this young ice regime, although with thick and old ice generally ≥ 1 standard deviation above the mean (An exception is the amount of ice older than ~ 2 years in 2020, which is very close to the mean). Further analysis (Supplementary Fig. S1) indicates that many years in the young ice regime show small secondary

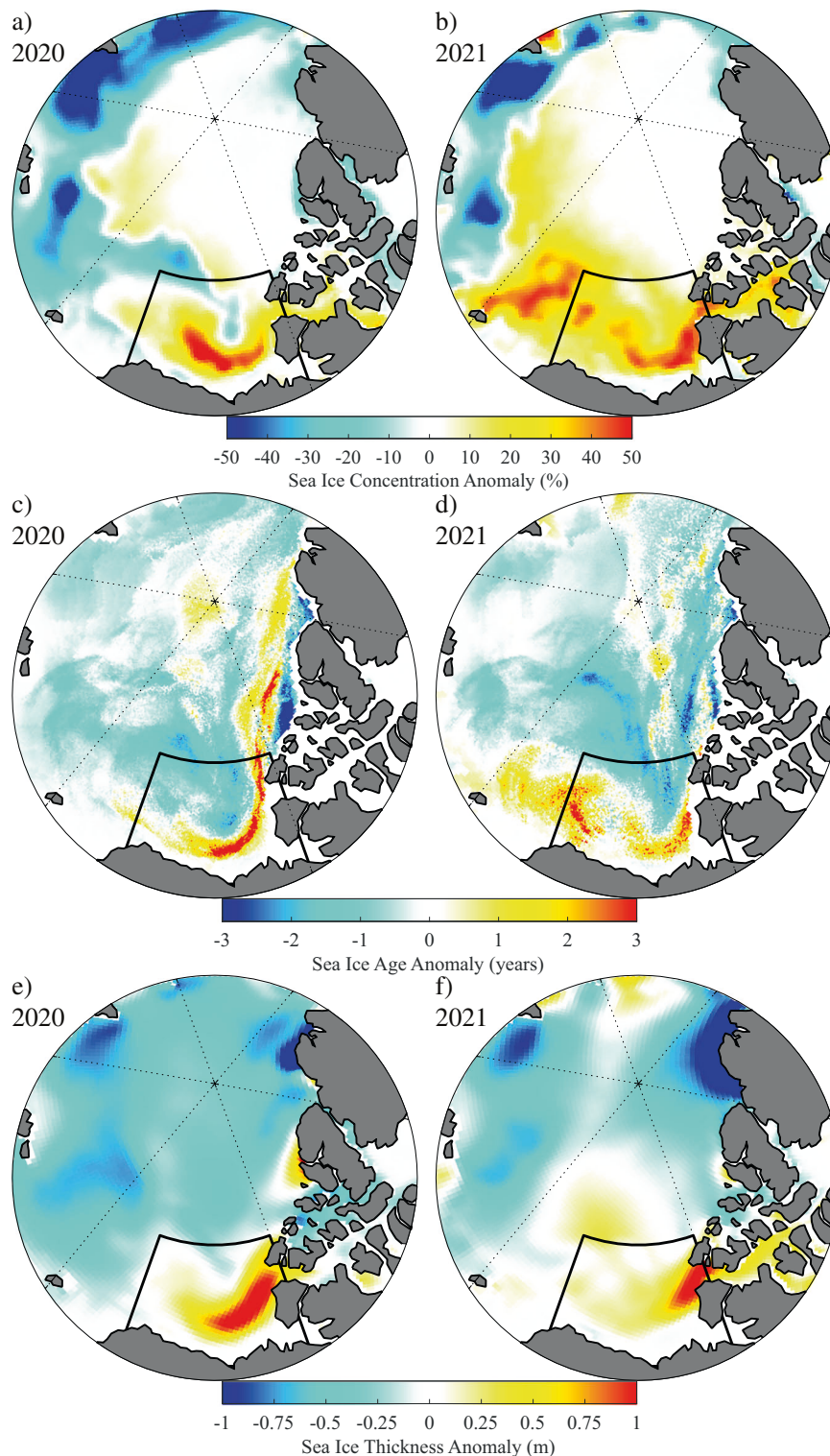


Fig. 1 Recent characteristics of summer (July–September) sea ice in the Western Arctic. Anomalies in the: NSIDC CDR sea ice concentration dataset for: **a** 2020 and **b** 2021; in the NSIDC sea ice age age dataset for: **c** 2020 and **d** 2021; in the PIOMAS sea ice thickness dataset for: **e** 2020 and **f** 2021. Anomalies are with respect to 2007–2019. The polygon indicates the region along the Beaufort Coast over which statistics were computed.

peaks of thick or old ice (such as seen in the 2021 thickness distribution between 1.5 and 2 m). These “long-tailed” thickness and age distributions are similar to that found in summer 2020 in the Wandel Sea¹. Thus, it seems that the Beaufort Sea is now dominated by thin, young ice, but a substantial component of thick, old ice remains. In the following sections, we examine the advective origins of this thick, old ice.

Impact of sea ice transport on the observed anomalies during the summers of 2020 and 2021. Recent work^{23–25} has emphasized the role that sea ice mass transport plays in determining the characteristics of pack ice in the Beaufort Sea. This transport can be decomposed into contributions from ice motion and from ice thickness; the seasonal climatology of these constituents as well as conditions during 2019/2020 and 2020/2021 are shown in Fig. 5.

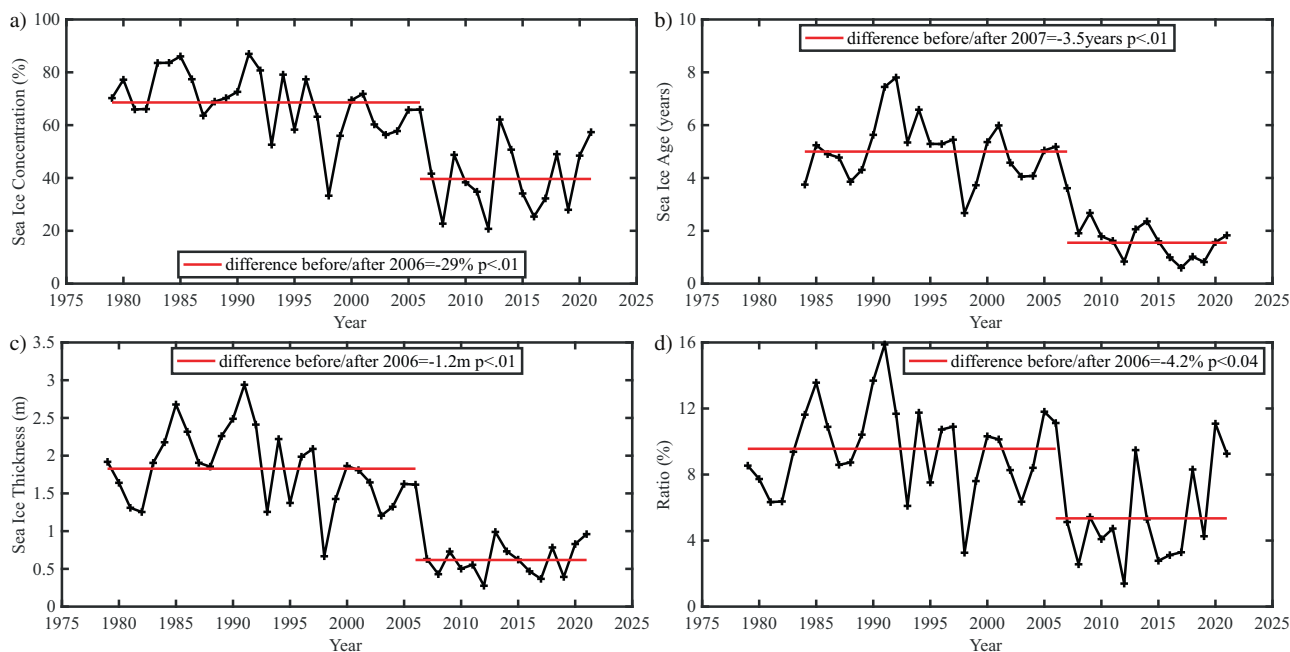


Fig. 2 Characteristics of summer (July–September) Beaufort Sea ice. Time series of the: **a** sea ice concentration (%) from the NSIDC CDR dataset 1979–2021; **b** sea ice age (years) from the NSIDC dataset 1984–2021; **c** sea ice thickness (m) from PIOMAS 1979–2021 and **d** ratio of the volume of Beaufort sea ice to Arctic sea ice from PIOMAS 1979–2021. In all cases, the red lines represent the step function fit with the specified breakpoint that minimizes the root-mean square error in the fit. The statistical significance of the step is indicated in the legend.

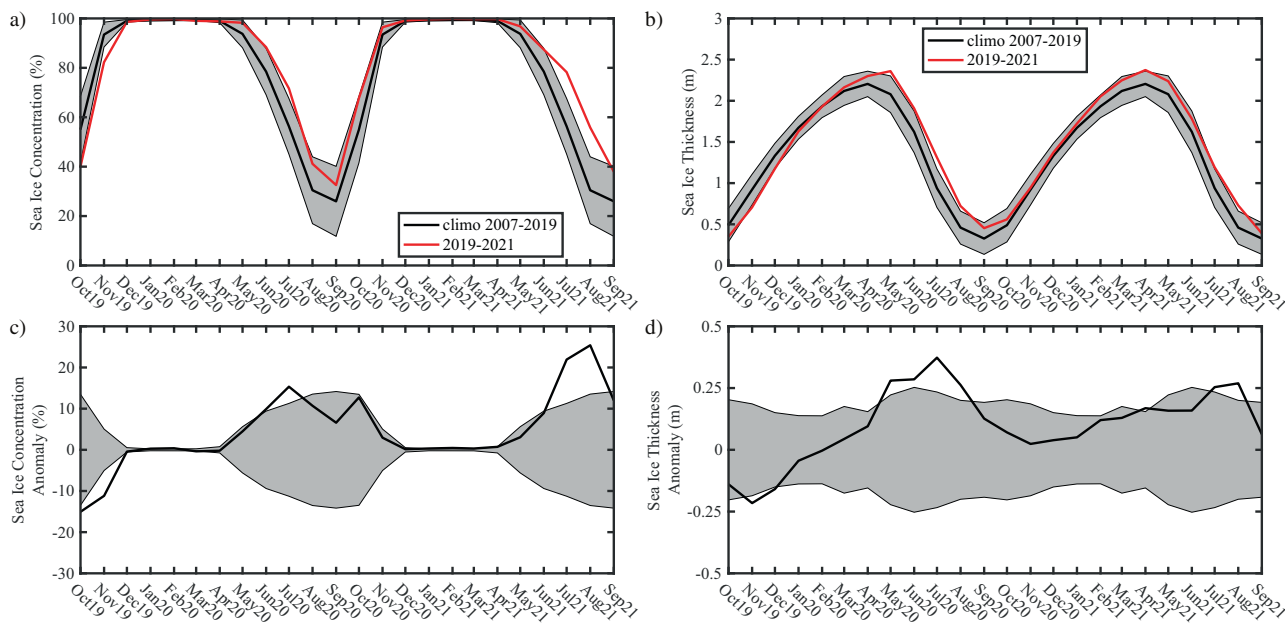


Fig. 3 Monthly mean Beaufort Sea ice characteristics from October 1 2019–September 30 2021. Time series (red curves) of the **(a)** monthly mean sea ice concentration (%) from the NSIDC CDR dataset and **(b)** monthly mean sea ice thickness (m) from PIOMAS with the climatological monthly mean values shown in black with one standard deviation above/below the mean indicated by the shading. The climatology is based on 2007–2019. In **(c)** and **(d)**, the corresponding anomalies are shown with the shading representing \pm one standard deviation.

The climatology (Fig. 5a–d) indicates the presence of a seasonally varying anticyclonic Beaufort Gyre in the western Arctic as well as the presence of the thickest ice along the northern coast of Greenland and the Canadian Arctic Archipelago, i.e., the LIA. The spatial extent of the Beaufort Gyre is largest during the cool season, defined as fall (OND), winter (JFM) and spring (AMJ) when there is transport of ice from the LIA into the Beaufort Sea as well as transport of ice out of the Beaufort Sea into the Chukchi

Sea. During summer (JAS), the Beaufort Gyre shrinks to only fill the Beaufort Sea.

The situation during 2019/2020 (Fig. 5e–h) differs markedly from the climatology. During fall 2019 (Fig. 5e), the Beaufort Gyre was displaced southwestward with a small region of cyclonic ice motion at the boundary between the Chukchi and Beaufort Seas. Consistent with the collapse of the Beaufort High during winter 2020²⁶, ice motion during this period (Fig. 5f) is generally eastward

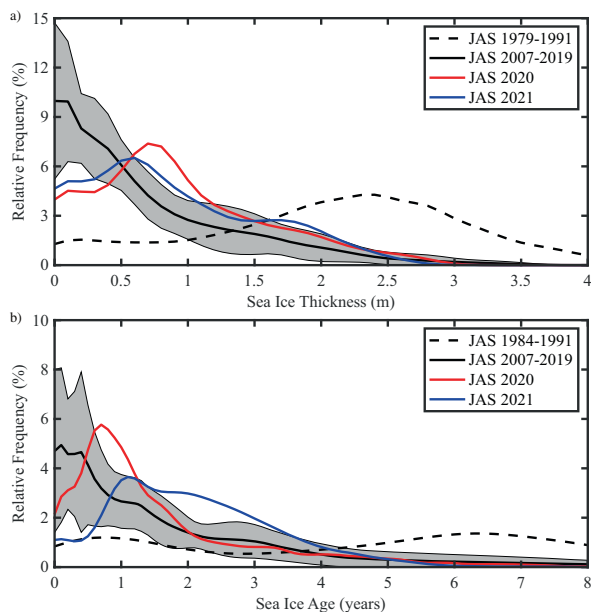


Fig. 4 Frequency distribution of summer (July–September) sea ice characteristics in the region of interest. **a** PIOMAS sea ice thickness distribution and **b** NSIDC sea ice age distribution. Climatological distributions for 1979–1991 (1984–1991 for ice age) and 2007–2019 are shown as well as distributions for 2020 and 2021. The shading represents one standard deviation above/below the 2007–2019 mean.

in the Beaufort Sea and largely cyclonic over the entire Arctic Ocean. This results in ice transport from the Chukchi Sea into the Beaufort Sea and even beyond, i.e., into the LIA. In spring 2020 (Fig. 5g), transport continued from the Beaufort Sea to the LIA, although the Chukchi-to-Beaufort transport abated. By summer 2020, ice motion had reverted toward climatology (Fig. 5h).

Conditions during 2020/2021 (Fig. 5i–l) were closer to climatology as compared to 2019/2020, although with some differences. Most notably during fall 2020 (Fig. 5i), the transport of thick, old ice from the LIA was restricted to a narrow region along the coast of the Canadian Arctic Archipelago, which appears to be linked to the presence of thick ice in the eastern Beaufort Sea. As discussed previously²³, this strong transport continued into winter 2021 (Fig. 5j), although its width increased and thus broadly impacted the northeastern Beaufort Sea. There was also strong westward transport out of the Beaufort into the Chukchi Sea.

Figure 6 shows the anomalies in sea ice motion, mass convergence, and thickness for the winters of 2020 and 2021 as well as the anomalies in sea-level pressure and 10 m wind fields for the same periods. The contrast in ice motion and sea ice thickness between the two winters is striking. During winter 2020 (Fig. 6a), anomalous cyclonic ice motion is evident as well as anomalously thick sea ice against Banks Island caused by convergence forced by eastward motion at this time (Fig. 6c, which actually started in fall 2019, Fig. 5f). Convergence also extends from the eastern Beaufort into the western LIA, where it acts to counter the long-term thinning trend; the result is enhanced negative ice thickness anomalies. This is supported by a comparison with winter 2021 (Fig. 6b, d), when thickness anomalies were much more negative and ice motion in the western LIA was closer to climatology, i.e., weakly divergent. Comparison of ice motion and thickness fields in the winters of 2020 and 2021 (Supplementary Fig. S2) demonstrates that the differences between these 2 years extend all the way from the Chukchi and Beaufort Seas into the western LIA.

The atmospheric circulation anomalies for these two winters highlight the role that sea-level pressure plays in forcing ice

motion. During winter 2020 (Fig. 6e), the collapse of the Beaufort High²⁶ resulted in lower sea-level pressures across the Arctic Ocean associated with a minimum 16 mb lower than climatology centered over the Barents Sea. Associated with this collapse, a cyclonic surface wind anomaly was present across the Arctic Ocean with a particularly high amplitude across the western boundary of the Beaufort Sea. In contrast, winter 2021 (Fig. 6f) was characterized by higher sea-level pressure over the Arctic Ocean with a maximum anomaly of 8 mb over the Barents Sea. As a result of this pressure perturbation, wind speeds were higher over the Arctic Ocean but did not reach the magnitudes observed during winter 2020.

Quantifying the role of ice transport in anomalous Beaufort Sea ice conditions during the winters of 2019/2020 and 2020/2021. Ice area and volume fluxes provide a way to quantify the transport of sea ice³⁰. Figure 7 shows the cumulative fluxes across the boundaries of the Beaufort Sea (as defined in Fig. 1) from October 1 through the following June 1 for 2019/2020, 2020/2021, as well as a climatology for the first 13 years of the young ice period 2007–2019. Positive values indicate a flux into the region. Daily PIOMAS ice motion and ice thickness data were used to calculate these fluxes. The ice area fluxes were also computed using the NSIDC ice motion data³¹ with similar results obtained (Supplementary Fig. S3).

We first consider the northern boundary. The ice area and volume fluxes across this boundary are relatively small in the climatology (Fig. 7a, b), with interannual variability that includes some years in which the fluxes are negative, i.e., from the Beaufort Sea toward the LIA. During the period from October to January in 2019/2020 as well as in 2020/2021, ice area and volume fluxes are positive and growing, at rates near or above the climatological mean, indicating intensifying ice transport into the Beaufort Sea. After January, the 2 years differ. In winter 2020 the cumulative fluxes plateau, indicating near-zero values in contrast to the climatology which continues to grow. Then in spring 2020 the fluxes turn strongly negative, with values of one or more standard deviation below the mean, implying an export of ice from the Beaufort Sea into the LIA. In fact, the cool season 2019/2020 ends with an unusually large net export of ice volume from the Beaufort into the LIA. The following year, we see that the fluxes in winter 2021 continue to intensify at about 1 standard deviation above the mean. Then in spring the cumulative fluxes decline back toward the climatological mean, with end-of-cool-season values near the climatological young ice regime mean of net transport from the LIA into the Beaufort.

At the western boundary, climatological ice area and ice volume fluxes are both directed out of the Beaufort Sea and into the Chukchi Sea (Fig. 7c, d). Although interannual variability is higher than that at the northern boundary, the fluxes are typically always negative. This is what makes the 2019/2020 area and volume fluxes so remarkable, in that they are nearly zero through winter 2020, and then turn strongly positive in spring, with values at or exceeding the mean by more than one standard deviation throughout the entire period. These positive fluxes reflect strong ice import from the west (Fig. 5f). In contrast, the fluxes in 2020/2021 became large and negative by early winter (greater than 1 standard deviation from the climatological mean), although this moderates later in the winter and spring. In this year, fluxes were strongly westward, from the Beaufort into the Chukchi Sea.

The sum of the fluxes across the two boundaries provides a measure of the net transport into the Beaufort Sea (Fig. 7e, f). The climatology indicates that the net ice area and volume fluxes are negative, indicating a loss of ice from the Beaufort Sea. This reflects the fact that the transport out of the region through the western

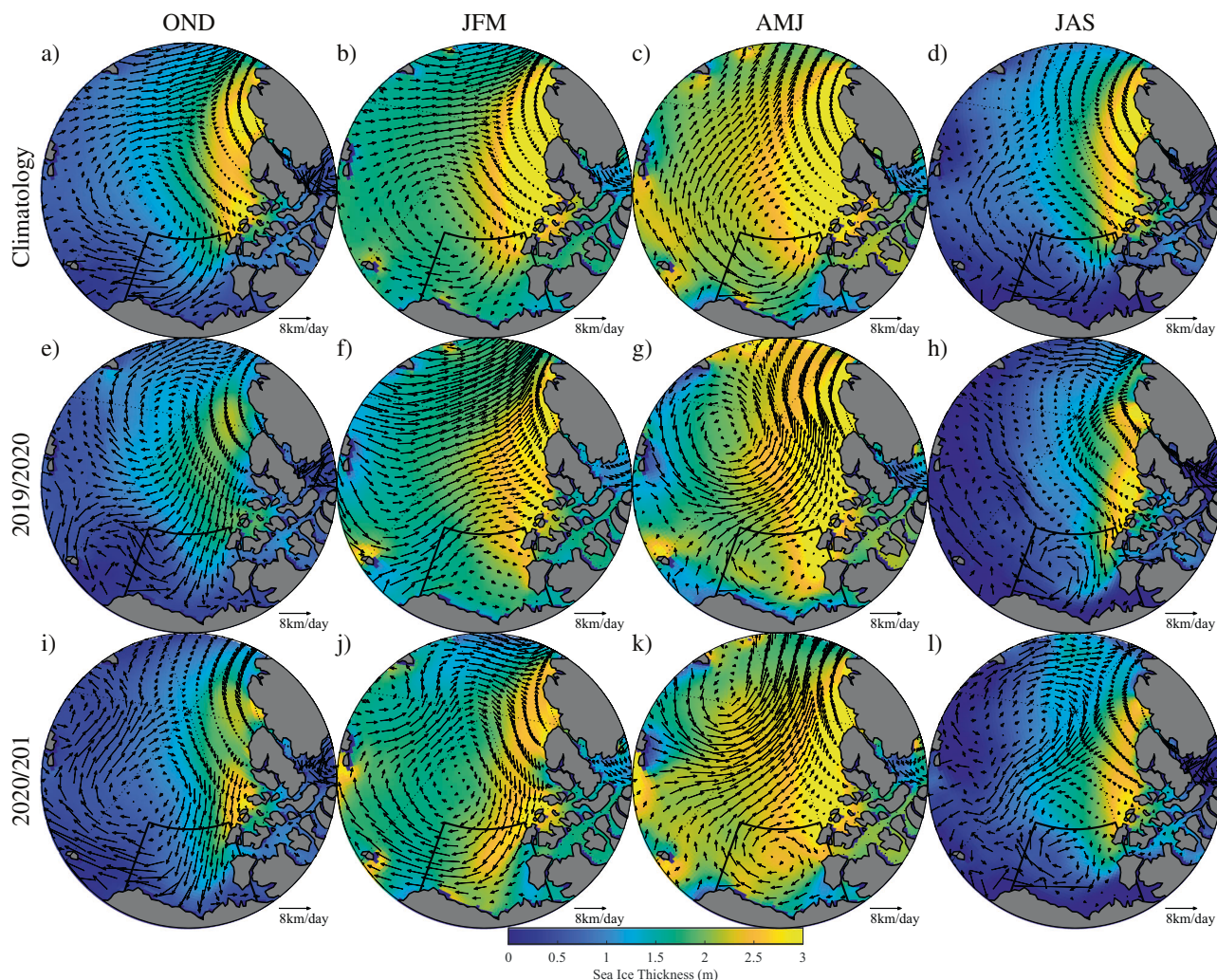


Fig. 5 Annual cycle in seasonal mean (OND: October–December; JFM: January–March; AMJ: April–June; JAS: July–September) sea ice thickness (shading - m) and sea ice motion (vectors- km/day). Results are shown for climatology (a–d) as well as 2019/2020 (e–h) and 2020/2021 (i–l). The polygon indicates the region along the Beaufort Coast over which statistics were computed. All fields are from PIOMAS.

boundary usually exceeds the transport into the region through the northern boundary. In this context, the net fluxes during 2019/2020 again stand out as remarkable, since they are strongly positive (i.e., net transport into the Beaufort), especially for ice area flux. The net fluxes during 2020/2021 are closer to climatological values, and are well within the range of climatological variability.

Impact of cool season ice fluxes on Beaufort Sea summer ice conditions. In this section, we seek to quantify how the cool-season sea ice transport into the Beaufort Sea impacts ice conditions in the following summer using two metrics. The first metric is Beaufort Sea ice volume (i.e., the product of ice thickness and ice concentration²⁷) on June 1. Even though melt can occur in parts of the study region prior to the beginning of June³², it is nevertheless a useful date for the start of the melt season. Our second metric is Beaufort Sea area-mean ice concentration during September, a measure of ice conditions at the end of the melt season and a closely observed indicator of climate change^{33,34}.

In Fig. 8, we correlate the net ice volume flux over the cool season, i.e., the period from October 1 to June 1 of the following year, against the Beaufort Sea June 1 ice volume anomaly, calculated by detrending the time series using a step function in 2007 that takes into account the changes between the new and old

ice regimes (Fig. 2). The ice volume flux does not exhibit any trend and so no detrending was done for this time series. The correlation was done for both the old and young ice regimes. For both periods, there is a statistically significant linear relationship showing that larger net cool season ice transport into the Beaufort Sea leads to larger ice volume anomalies on June 1. However, the larger spread in the data for the old ice regime leads to a smaller percentage of the variance explained by ice transport, ~14%, as compared to ~45% for the young ice regime. The statistics are similar if May 1 is used as the end of the cool season, although using April 1 degrades the relationship to statistical insignificance, consistent with the springtime “predictability barrier”³⁵ that arises from late-winter variability in ice-dynamics and ice growth.

Regarding conditions at the end of the summer, it seems intuitive that ice retreat might be slowed by the presence of thick ice. Indeed, discussions in the popular press⁵ have speculated that thick ice contributed to the relatively moderate September 2021 sea ice extent (12th lowest on record and the highest since 2014). On the other hand, it has also been suggested that cool atmospheric conditions during the summer of 2021 contributed to this relative maxima in sea ice extent³⁶.

To explore this question, we correlate PIOMAS-derived Beaufort Sea ice volume on June 1 with NSIDC CDR-derived

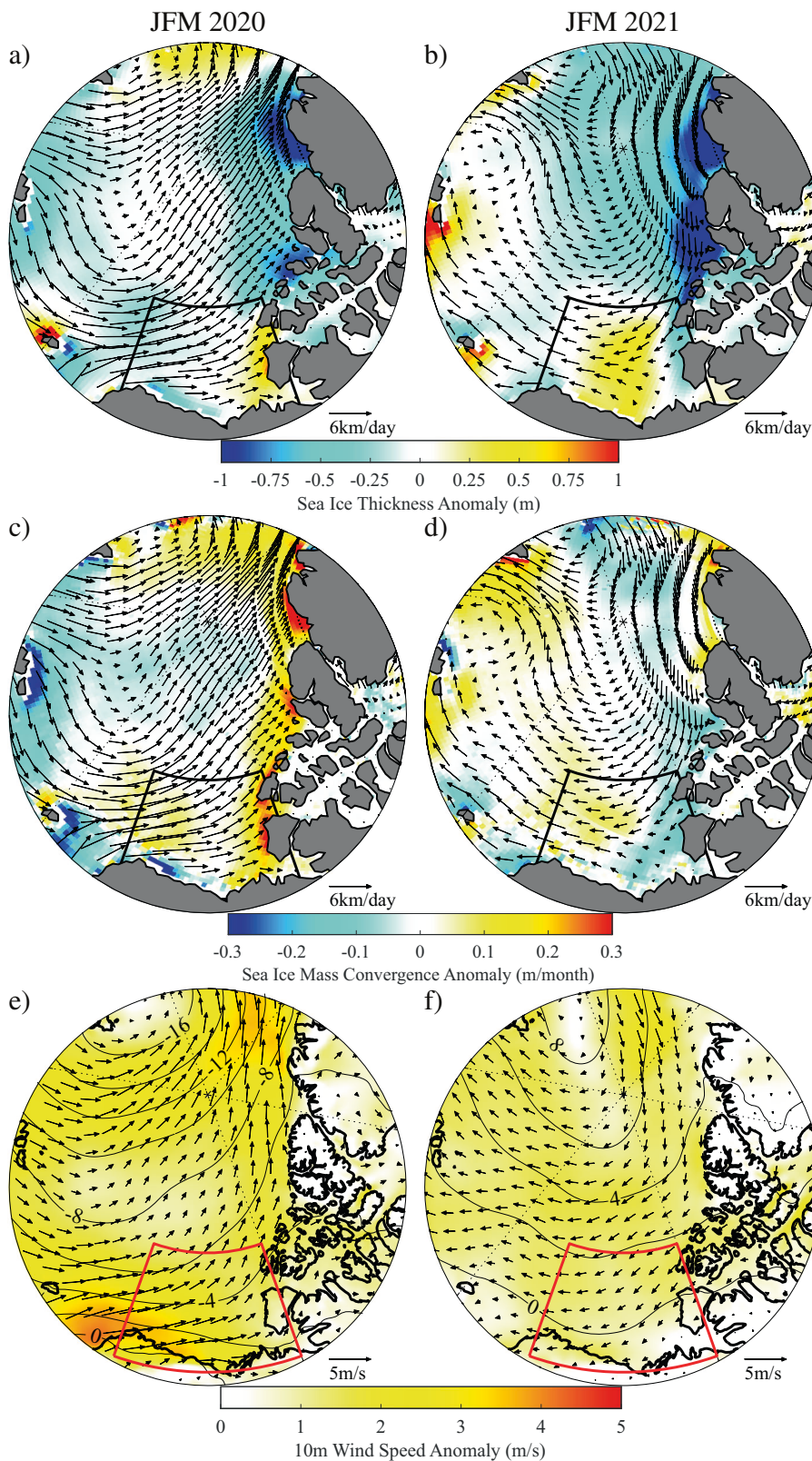


Fig. 6 Anomalous nature of the winter (JFM) sea ice and atmospheric circulation during 2020 and 2021. Sea ice thickness (shading - m) and sea ice motion (vectors- km/day) anomalies with respect to climatology (2007–2019) for: **a** 2020 and **b** 2021. Sea ice mass convergence (shading - m/month) and sea ice motion (vectors- km/day) anomalies with respect to climatology (2007–2019) for: **c** 2020 and **d** 2021. Sea-level pressure (contours - mb), 10 m wind (vectors- m/s) and 10 m wind speed (shading-m/s) anomalies with respect to climatology (1979–2021) for: **e** 2020 and **f** 2021. The polygon indicates the region along the Beaufort Coast over which statistics were computed. Sea ice fields are from PIOMAS. Atmospheric fields are from ERA5.

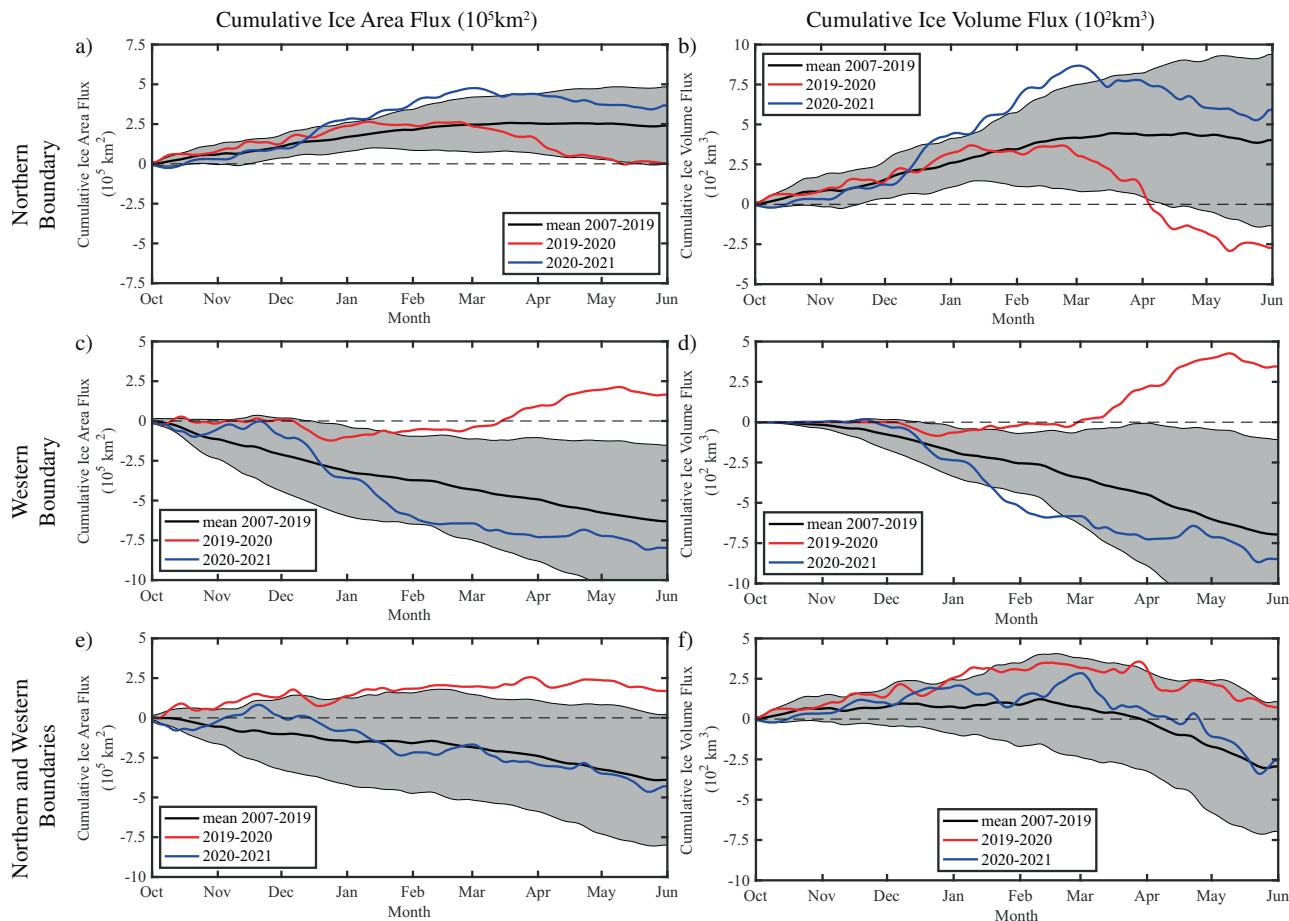


Fig. 7 Variability in the PIOMAS sea ice fluxes into the region of interest. Cumulative: **a** ice area (10^5 km^2) flux and **b** ice volume flux (10^2 km^3) through the northern boundary of the region of interest. Cumulative: **c** ice area (10^5 km^2) flux and **d** ice volume flux (10^2 km^3) through the western boundary of the region of interest. The net cumulative: **e** ice area (10^5 km^2) flux and **f** ice volume flux (10^2 km^3) through the northern and western boundaries of the region of interest. Results are shown for climatology (2007–2019) as well as for 2019–2020 and 2020–2021 with the shading representing \pm one standard deviation above/below the climatological mean. Positive fluxes are into the region of interest.

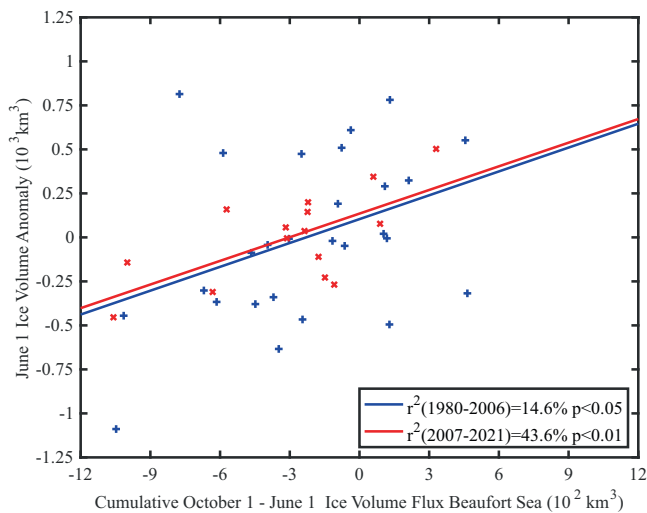


Fig. 8 Relationship between cumulative cool season ice volume flux into the Beaufort Sea region and June 1 Beaufort Sea ice volume 1980–2021. Scatterplot of the cool season (October 1 - June 1 following year) PIOMAS ice volume flux and June 1 PIOMAS ice volume anomaly. Linear least squares fit to the data for the two regimes are also shown as are the percentage of the variance explained. The ice volume time series has been detrended by step functions with a breakpoint in 2007.

September-mean sea ice concentration³⁷. Given the nature of the underlying time series (Fig. 2), we have used step functions with a breakpoint in 2007 to detrend the data (see Materials and Methods). Although there is considerable spread, Fig. 9 indicates that there is a statistically significant linear relationship, with June 1 ice volume accounting for just under 40% of the variability in ice concentration during September for both the old and new ice regimes. Similar results are obtained if one uses the PIOMAS sea ice concentration during September (Supplementary Fig. S4).

A next logical step might be to link these two correlations together and ask, How does cool season ice transport impact end-of-summer ice concentration? Given the above results, assuming that there are no other factors related to cool season transport that impact summer ice melt and the cascade of probabilities, one would expect that the former would explain $\sim 5\%$ and $\sim 16\%$ of the variability in the latter for the old and new ice regimes. The results shown in Supplementary Fig. S5 confirm these assumptions; however, we also find that this relationship is not statistically significant in either regime.

Discussion

This paper is motivated by an interest in understanding the processes responsible for the large extent of thick and old sea ice present in the Beaufort Sea during the summers of 2020 and 2021 (Fig. 1). Our results confirm earlier work⁶ and indicates that the Beaufort Sea underwent a transition around 2007 in its summer ice

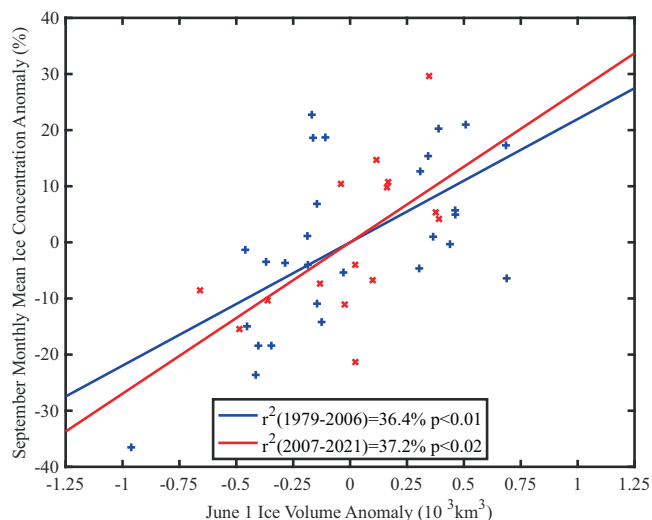


Fig. 9 Relationship between June 1 ice conditions and September mean ice concentration 1979–2021. Scatterplot of the June 1 PIOMAS ice volume anomaly and the NSIDC CDR September monthly mean ice concentration anomaly. Linear least squares fit to the data for the two regimes are also shown as are the percentage of the variance explained. Both time series have been detrended by step functions with a breakpoint in 2007.

characteristics (Fig. 2). Prior to this transition, the summer Beaufort Sea ice thickness distribution was characterized by a multi-year thick ice mode between 2 and 2.5 m, with long tails toward both thinner and thicker ice. However, more recently this distribution has a mode well below 0.5 m and considerably thinner ice (Fig. 4). A step function-like increase in the kinetic energy of Beaufort Gyre was also observed to occur around 2007³⁸ that has been suggested to be associated with the loss of sea ice³⁹.

Nonetheless, recent ice thickness distributions have contributions from thick ice that sometimes even exhibit a secondary mode at 2–2.5 m (Fig. 4). In particular, the Beaufort Sea in the summers of 2020 and 2021 contributed approximately 10% of total Arctic ice volume, a doubling of the mean value over 2007–2021, and on par with contributions prior to 2007 (Fig. 2d). We argue that advection during the previous cool season contributed to the presence of thicker and older summer ice during 2020 and 2021, but that the advective mechanisms were very different in these 2 years. In particular, winter and spring 2020 were characterized by a collapse of the Beaufort High²⁶ that caused the Beaufort Gyre to reverse resulting in cyclonic ice motion across the Arctic Ocean (Fig. 5f, g), an event first reported to have occurred during the winter of 2017²⁴. The sea-level pressure anomaly responsible for this collapse was centered over the Barents Sea (Fig. 6a). This reversal of the normal anticyclonic ice motion transported ice from the Chukchi Sea into the Beaufort Sea and then into the western LIA (Fig. 6a), which contributed to the presence of thick sea ice in the eastern Beaufort Sea and western LIA (Fig. 1c, e).

The conditions leading up to summer 2021 were markedly different. There was enhanced anticyclonic ice motion across the Arctic during fall 2020 and winter 2021 (Fig. 5i, j) which was associated with positive sea-level pressure anomalies that were largest in the eastern Arctic (Fig. 6d). The importance of higher sea-level pressures in the western Arctic during December 2020 to February 2021 as a contributor to the enhanced transport of sea ice into the Beaufort Sea from the LIA has been previously noted²³ and confirmed by the results in Fig. 7. We also emphasize that sea-level pressure anomalies during winter 2021 were largest in the eastern Arctic and it was this ridge that contributed to the

anomalously strong winds and ice transport into the Beaufort Sea from the LIA and then to the Chukchi Sea (Fig. 6b, d).

Figure 1 clearly shows the presence of extensive regions of thick and old Beaufort sea ice during the summers of 2020 and 2021. Given that over the cool season of 2019/2020, there was advection of thinner and younger ice from the Chukchi into the Beaufort, how can one explain the presence of old ice during summer 2020? We believe that the collapse of the Beaufort High during the preceding cool season and the concomitant ice motion reversal trapped old ice that would have normally exited the Beaufort into the Chukchi. The reversal also led to thicker ice as a result of convergence against Banks Island (Fig. 1e) This distinction is consistent with the presence in summer 2020 of anomalous thick ice (Fig. 4a) but near-climatological mean ice age (Fig. 4b).

As previously noted, the summer of 2020 was characterized by a dipole in sea ice characteristics across the Wandel and Beaufort Seas, i.e., low concentration, age, and thickness in the former and high values in the latter. At the end of the preceding cool season, both regions were characterized by the presence of thick ice that was the result of anomalous ice advection associated with the collapse of the Beaufort High (Fig. 6a, c, e). The different trajectories that resulted in a summer minimum in the Wandel Sea and a summer maximum in the Beaufort Sea were the result of thermodynamic and dynamic processes active during the summer.

We have shown that Beaufort Sea ice volume at the start of the melt season is proportional to the cool season net ice volume flux into the region, especially in recent years (Fig. 8). Prior to 2007, Beaufort Sea ice was generally thicker and so transport into the region (largely from the LIA) did not have a large impact on the region's ice volume. In the new thin ice regime, this transport now plays a greater role in the region's ice volume.

There is an ongoing debate as to the importance of ice thickness anomalies during the preceding cool season versus warm season atmospheric variability on summer sea ice extent^{5,36}. Our results indicate that June 1 Beaufort Sea ice volume anomalies account for approximately 40% of the variance in the following September mean ice concentration. However, a statistically significant relationship linking cool-season sea ice volume transport into the region and the following September mean ice concentration does not emerge from our results.

As sea ice becomes more mobile owing to general Arctic sea ice thinning^{4,40}, the large-scale advection anomalies studied here may become more common. This may lead to enhanced inter-annual variability in Beaufort Sea ice conditions, which will likely have impacts on marine infrastructure⁴¹, shipping⁴², ecosystems, and ice-dependent species. For example, polar bears prefer annual sea ice as it generally occurs over productive waters over the continental shelf. This rich environment allows polar bears to gain enough weight in spring to survive a fasting period during the ice-free season, when they largely live off their fat reserves until the ice forms the following year⁴³. Long-term loss of annual sea ice is leading to longer open water seasons⁴⁴ and numerous studies show these trends are negatively impacting polar bears. Multi-year ice advected into an otherwise ice-free area may have transient benefits for polar bears, if they are able to utilize large floes for opportunistic foraging. Opportunities to obtain even a small number of seals during the fasting season have the potential to impact both survival and reproduction⁴⁵. At the same time, redistribution of bears during summer with presence of MY ice may impact subpopulation assessments designed around the low-ice season to maximize detections of bears⁴⁶.

Methods

The Beaufort Sea domain. For the purposes of this paper, we define the western and eastern limits of the Beaufort Sea by 160°W and 120°W and the northern limit by 78°N. The southern limit is defined by the coastline of Alaska and the Yukon

and Northwest Territories. Please refer to the polygon in Fig. 1 and some subsequent figures. Similar definitions of the Beaufort Sea have been used by other authors^{21,23}. The results identified in this paper were not sensitive to small changes in the definition of the domain.

The PIOMAS model. The Pan-Arctic Ice Ocean Modeling and Assimilation System (PIOMAS) is a coupled ice ocean modeling and data assimilation system⁴⁷. It consists of coupled sea ice and ocean models that are forced by atmospheric fields from the NCEP Reanalysis⁴⁸. The sea ice model employs a multi-category thickness and enthalpy distribution⁴⁹ as well as a teardrop viscous plastic rheology⁵⁰. The ocean model is the Parallel Ocean Program (POP) model⁵¹, which has 30 vertical levels of varying thicknesses that resolve both surface layers and bottom topography.

PIOMAS employs a generalized orthogonal curvilinear coordinate system with the “North Pole” displaced over Greenland and a mean horizontal resolution of approximately 30 km. To provide lateral boundary conditions, the model is one-way nested within a global version of the same model⁴⁷.

PIOMAS assimilates satellite sea ice concentration and sea surface temperature data and is calibrated and validated with all available in-situ and remotely-sensed sea ice thickness and draft data^{27,47,52} as well as in-situ sea ice motion data from buoys^{53,54}.

Sea ice concentration. For sea ice concentration, we use the National Snow and Ice Data Center – Climate Data Record (NSIDC-CDR). This dataset is derived from passive microwave satellite data with a retrieval that is a merging of the NASA Team and NASA Bootstrap algorithms³⁷. The data is available from 1979 onwards at horizontal resolution of 25 km. The data is available every 3 days up to 1984 and daily afterwards.

Sea ice motion and age. The sea ice motion dataset³¹ blends passive microwave, visible and infrared satellite data along ice buoy data and winds from the NCEP Reanalysis⁴⁸ to provide an estimate of ice motion. The data is available every 3 days up to 1984 and on a daily basis afterwards at a spatial resolution of 12.5 km. The sea age dataset⁵⁵ provides an estimate of the age of sea ice up to ~15 years of age by tracking the motion of contiguous areas of sea ice using the NSIDC’s sea ice motion dataset³¹.

Atmospheric reanalysis. The ERA5 reanalysis⁵⁶ is used to characterize atmospheric motion. It assimilates all available data from land stations, ocean and sea ice buoys, radiosonde data as well as satellite data into a frozen version of the data assimilation system from European Center for Medium Range Forecasting’s Integrated Forecasting Center. It is available on an hourly basis at a horizontal resolution of ~25 km from 1979-onwards. The 10 m winds and sea-level pressure fields from the ERA5 were used in this study.

Fitting of data. Given the rapid warming that the Arctic is experiencing, most environmental parameters are characterized by large changes. A number of different methods have been used to quantify these changes. The most common approach is based on the assumption that the changes can be characterized by a linear trend obtained by a linear least squares fit to the observed data³⁴. However, there is evidence that the changes are not uniform in time and piecewise linear fits have also been used⁵⁷. A challenge with this approach is the selection of the breakpoint. Comiso et al.⁵⁷ did not provide a rationale for their choice of breakpoint. Moore et al.²⁸ used a low frequency fit to the data derived using Singular Spectral Analysis (SSA) to identify the breakpoint in time series of Greenland and Iceland Sea heat flux time series. Moore et al.⁵⁸ used a more reproducible technique that selected the breakpoint of a paleoproxy for Labrador Sea ice conditions through the minimization of the root mean-square (rms) error based on all possible breakpoints. There is however evidence that changes may be nonlinear in nature and are better characterized by step function changes^{38,59}.

The choice of the paradigm to characterize the change (linear, piecewise linear and step function) is not always evident. In this paper, we took an agnostic approach and apply all three paradigms and for all possible breakpoints, selecting the one that minimizes the rms error. The step function fits, with breakpoints in either 2006 or 2007, for all metrics all have root-mean square errors that are smaller than respective linear fits as well as all piecewise linear fits.

Data availability

The PIOMAS data is available from the University of Washington’s Polar Sciences Center and can be accessed at: http://psc.apl.uw.edu/research/projects/arctic-sea-ice-volume-anomaly/data/model_grid.

The NSIDC ice age data is available from the National Snow and Ice Data Center and can be accessed at: <https://nsidc.org/data/NSIDC-0611/versions/4>

The NSIDC ice concentration data is available from the National Snow and Ice Data Center and can be accessed at: <https://nsidc.org/data/G02202/versions/3>

The NSIDC ice motion data is available from the National Snow and Ice Data Center and can be accessed: <https://nsidc.org/data/nsidc-0116/versions/4>

The ERA5 reanalysis data is available from the Copernicus Climate Data Store and can be accessed at: <https://cds.climate.copernicus.eu/cdsapp#/dataset/reanalysis-era5-single-levels>.

Received: 8 November 2021; Accepted: 9 August 2022;

Published online: 30 August 2022

References

- Schweiger, A. J., Steele, M., Zhang, J., Moore, G. & Laidre, K. L. Accelerated sea ice loss in the Wandel Sea points to a change in the Arctic’s Last Ice Area. *Commun. Earth Environ.* **2**, 1–11 (2021).
- Newton, R., Pfirman, S., Tremblay, L. B. & DeRepentigny, P. Defining the ‘ice shed’ of the Arctic Ocean’s Last Ice Area and its future evolution. *Earth’s Futur.* e2021EF001988. <https://doi.org/10.1029/2021EF001988> (2021).
- Pfirman, S., Fowler, C., Tremblay, L. B. & Newton, R. The last Arctic Sea ice refuge. *Circle* **4**, 6–8 (2009).
- Moore, G. W. K., Schweiger, A., Zhang, J. & Steele, M. Spatiotemporal variability of sea ice in the arctic’s last ice area. *Geophys. Res. Lett.* **46**, 11237–11243 (2019).
- Fountain, H. Arctic Sea ice hits annual low, but it’s not as low as recent years, *New York Times*, September 23.
- Wood, K. R. et al. Is there a “new normal” climate in the Beaufort Sea? *Polar Res.* **32**, <https://doi.org/10.3402/polar.v32i0.19552> (2013).
- Arrigo, K. R. et al. Massive phytoplankton blooms under Arctic sea ice. *Science* **336**, 1408–1408 (2012).
- Arrigo, K. R. et al. Phytoplankton blooms beneath the sea ice in the Chukchi Sea. *Deep Sea Res. Part II Top. Stud. Oceanogr.* **105**, 1–16 (2014).
- Assmy, P. et al. Leads in Arctic pack ice enable early phytoplankton blooms below snow-covered sea ice. *Sci. Rep.* **7**, 1–9 (2017).
- Mundy, C. et al. Contribution of under-ice primary production to an ice-edge upwelling phytoplankton bloom in the Canadian Beaufort Sea. *Geophys. Res. Lett.* **36**, 1–5 (2009).
- Mundy, C. J. et al. Role of environmental factors on phytoplankton bloom initiation under landfast sea ice in Resolute Passage, Canada. *Marine Ecol. Progress Series* **497**, 39–49 (2014).
- Laidre, K. L. et al. Transient benefits of climate change for a high-Arctic polar bear (*Ursus maritimus*) subpopulation. *Global Change Biol.* **26**, 6251–6265 (2020).
- Atwood, T. C. et al. Rapid environmental change drives increased land use by an Arctic marine predator. *PLoS One* **11**, e0155932 (2016).
- Rode, K. D. et al. Spring fasting behavior in a marine apex predator provides an index of ecosystem productivity. *Global Change Biol.* **24**, 410–423 (2018).
- Pagano, A. M., Durner, G. M., Atwood, T. C. & Douglas, D. C. Effects of sea ice decline and summer land use on polar bear home range size in the Beaufort Sea. *Ecosphere* **12**, e03768 (2021).
- Rigor, I. G., Wallace, J. M., & Colony, R.L. Response of sea ice to the Arctic oscillation. *J. Clim.* **15**, 2648–2663 (2002).
- Serreze, M. C. & Barrett, A. P. Characteristics of the Beaufort Sea high. *J. Clim.* **24**, 159–182, <https://doi.org/10.1175/2010JCLI3636.1> (2010).
- Proshutinsky, A., Bourke, R. & McLaughlin, F. The role of the Beaufort Gyre in Arctic climate variability: Seasonal to decadal climate scales. *Geophys. Res. Lett.* **29**, 15-11-15-14 (2002).
- Petty, A. A., Hutchings, J. K., Richter-Menge, J. A. & Tschudi, M. A. Sea ice circulation around the Beaufort Gyre: The changing role of wind forcing and the sea ice state. *J. Geophys. Res. Oceans* **121**, 3278–3296 (2016).
- Maslanik, J. A., Serreze, M. C. & Agnew, T. On the record reduction in 1998 western Arctic sea-ice cover. *Geophys. Res. Lett.* **26**, 1905–1908 (1999).
- Babb, D., Landy, J., Barber, D. & Galley, R. Winter sea ice export from the Beaufort Sea as a preconditioning mechanism for enhanced summer melt: A case study of 2016. *J. Geophys. Res. Oceans* **124**, 6575–6600 (2019).
- Moore, G. W. K., Howell, S. E. L. & Brady, M. First observations of a transient polynya in the last ice area North of Ellesmere Island. *Geophys. Res. Lett.* 1–10, <https://doi.org/10.1029/2021GL095099> (2021).
- Mallett, R. et al. Record winter winds in 2020/21 drove exceptional Arctic sea ice transport. *Commun. Earth. Environ.* **2**, 1–6 (2021).
- Moore, G. W. K., Schweiger, A., Zhang, J. & Steele, M. Collapse of the 2017 winter Beaufort High: A response to thinning sea ice? *Geophys. Res. Lett.* 1–10, <https://doi.org/10.1002/2017GL076446> (2018).
- Babb, D. et al. The 2017 reversal of the Beaufort Gyre: Can dynamic thickening of a seasonal ice cover during a reversal limit summer ice melt in the Beaufort Sea? *J. Geophys. Res. Oceans* **125**, e2020JC016796 (2020).
- Ballinger, T. J. et al. Unusual west Arctic storm activity during winter 2020: Another collapse of the Beaufort High? *Geophys. Res. Lett.* **48**, e2021GL092518 (2021).

27. Schweiger, A. et al. Uncertainty in modeled Arctic sea ice volume. *J. Geophys. Res. Oceans* **116**, 1–21 (2011).
28. Moore, G. W. K., Våge, K., Pickart, R. S. & Renfrew, I. A. Decreasing intensity of open-ocean convection in the Greenland and Iceland seas. *Nat. Clim. Change* **5**, 877–882 (2015).
29. Bowman, A. W. & Azzalini, A. *Applied smoothing techniques for data analysis: the kernel approach with S-Plus illustrations*. Vol. 18 (OUP Oxford, 1997).
30. Kwok, R., Toudal Pedersen, L., Gudmandsen, P. & Pang, S. S. Large sea ice outflow into the Nares Strait in 2007. *Geophys. Res. Lett.* **37**, <https://doi.org/10.1029/2009GL041872> (2010).
31. Tschudi, M., Fowler, C., Maslanik, J., Stewart, J. S. & Meier, W. N. Polar Pathfinder daily 25 km EASE-Grid Sea Ice motion vectors, version 3. *National Snow and Ice Data Center Distributed Active Archive Center*, accessed February (2016).
32. Liu, Z. & Schweiger, A. Synoptic conditions, clouds, and sea ice melt onset in the Beaufort and Chukchi seasonal ice zone. *J. Clim.* **30**, 6999–7016 (2017).
33. Maslanik, J., Stroeve, J., Fowler, C. & Emery, W. Distribution and trends in Arctic sea ice age through spring 2011. *Geophys. Res. Lett.* **38**, <https://doi.org/10.1029/2011GL047735> (2011).
34. Parkinson, C. L. & Cavalieri, D. J. Arctic sea ice variability and trends, 1979–2006. *J. Geophys. Res. Oceans* **113**, C07003, <https://doi.org/10.1029/2007jc004558> (2008).
35. Bushuk, M., Winton, M., Bonan, D. B., Blanchard-Wrigglesworth, E. & Delworth, T. L. A mechanism for the Arctic sea ice spring predictability barrier. *Geophys. Res. Lett.* **47**, e2020GL088335 (2020).
36. Thompson, T. Arctic sea ice hits 2021 minimum. *Nature*, <https://doi.org/10.1038/d41586-021-02649-6> (2021).
37. Peng, G., Meier, W. N., Scott, D. J. & Savoie, M. H. A long-term and reproducible passive microwave sea ice concentration data record for climate studies and monitoring. *Earth Syst. Sci. Data* **5**, 311–318, <https://doi.org/10.5194/essd-5-311-2013> (2013).
38. Zhong, W., Zhang, J., Steele, M., Zhao, J. & Wang, T. Episodic extrema of surface stress energy input to the western Arctic Ocean contributed to step changes of freshwater content in the Beaufort Gyre. *Geophys. Res. Lett.* **46**, 12173–12182, <https://doi.org/10.1029/2019GL084652> (2019).
39. Armitage, T. W., Manucharyan, G. E., Petty, A. A., Kwok, R. & Thompson, A. F. Enhanced eddy activity in the Beaufort Gyre in response to sea ice loss. *Nat. Commun.* **11**, 1–8 (2020).
40. Spreen, G., Kwok, R. & Menemenlis, D. Trends in Arctic sea ice drift and role of wind forcing: 1992–2009. *Geophys. Res. Lett.* **38**, <https://doi.org/10.1029/2011GL048970> (2011).
41. Barber, D. G. et al. Climate change and ice hazards in the Beaufort Sea. *Elementa Sci. Anthropocene* **2**, <https://doi.org/10.12952/journal.elementa.000025> (2014).
42. Mudryk, L. R. et al. Impact of 1, 2 and 4 °C of global warming on ship navigation in the Canadian Arctic. *Nat. Clim. Change* **11**, 673–679, <https://doi.org/10.1038/s41558-021-01087-6> (2021).
43. Laidre, K. L. et al. Interrelated ecological impacts of climate change on an apex predator. *Ecological Applications* **30**, e02071 (2020).
44. Stern, H. L. & Laidre, K. L. Sea-ice indicators of polar bear habitat. *The Cryosphere* **10**, 2027–2041 (2016).
45. Laidre, K. L., Stirling, I., Estes, J. A., Kochnev, A. & Roberts, J. Historical and potential future importance of large whales as food for polar bears. *Frontiers in Ecology and the Environment* **16**, 515–524 (2018).
46. Bromaghin, J. F. et al. Polar bear population dynamics in the southern Beaufort Sea during a period of sea ice decline. *Ecological Applications* **25**, 634–651 (2015).
47. Zhang, J. & Rothrock, D. A. Modeling Global Sea Ice with a Thickness and Enthalpy Distribution Model in Generalized Curvilinear Coordinates. *Monthly Weather Review* **131**, 845–861 (2003).
48. Kalnay, E. et al. The NCEP/NCAR 40-year reanalysis project. *B Am Meteorol Soc* **77**, 437–471 (1996).
49. Zhang, J. & Rothrock, D. A thickness and enthalpy distribution sea-ice model. *Journal of Physical Oceanography* **31**, 2986–3001 (2001).
50. Zhang, J. & Rothrock, D. Effect of sea ice rheology in numerical investigations of climate. *Journal of Geophysical Research: Oceans* **110** (2005).
51. Smith, R., Dukowicz, J. & Malone, R. Parallel ocean general circulation modeling. *Physica D: Nonlinear Phenomena* **60**, 38–61 (1992).
52. Wang, X., Key, J., Kwok, R. & Zhang, J. Comparison of Arctic sea ice thickness from satellites, aircraft, and PIOMAS data. *Remote Sensing* **8**, 713 (2016).
53. Schweiger, A. J. & Zhang, J. Accuracy of short-term sea ice drift forecasts using a coupled ice-ocean model. *Journal of Geophysical Research: Oceans* **120**, 7827–7841 (2015).
54. Zhang, J., Lindsay, R., Schweiger, A. & Rigor, I. Recent changes in the dynamic properties of declining Arctic sea ice: A model study. *Geophysical Research Letters* **39**, <https://doi.org/10.1029/2012GL053545> (2012).
55. Tschudi, M., Meier, W., Stewart, J., Fowler, J. & Maslanik, J. EASE-Grid Sea Ice Age, Version 4, 2019).
56. Hersbach, H. et al. The ERA5 global reanalysis. *Quarterly Journal of the Royal Meteorological Society* **146**, 1999–2049, <https://doi.org/10.1002/qj.3803> (2020).
57. Comiso, J. C., Parkinson, C. L., Gersten, R. & Stock, L. Accelerated decline in the Arctic sea ice cover. *Geophysical Research Letters* **35**, <https://doi.org/10.1029/2007GL031972> (2008).
58. Moore, G., Halfar, J., Majeed, H., Adey, W. & Kronz, A. Amplification of the Atlantic Multidecadal Oscillation associated with the onset of the industrial-era warming. *Scientific Reports* **7**, 1–10 (2017).
59. Våge, K., Moore, G. W. K., Jónsson, S. & Valdimarsson, H. Water mass transformation in the Iceland Sea. *Deep Sea Research Part I: Oceanographic Research Papers* **101**, 98–109 (2015).

Acknowledgements

We would like to acknowledge support from the Natural Sciences and Engineering Research Council of Canada (GWKM), the World Wildlife Fund (G-1122-035-00-I, K.L.L., A.S., and J.Z.), NASA Cryosphere Program (NNX16AK43G, 80NSSC20K0134, 80NSSC18K0837, M.S.; NNX17AD27G and 80NSSC20K1253, A.S. and J.Z.), NSF Office of Polar Programs (PLR-1603266, OPP-1751363 M.S.; NSF-OPP-1744568, A.S.; NNA-1927785, J.Z.), and the Office of Naval Research (N00014-17-1-2545 M.S.; N00014-17-1-3162, A.S., J.Z.).

Author contributions

This work had critical contributions from all authors in developing the ideas, the analysis, as well as writing and review. G.W.K.M. took the lead in writing and conducted the analysis. M.S., A.J.S., J.Z., and K.L. contributed to the analysis and edited the manuscript. K.L. provided the perspective on the implications for marine mammals.

Competing interests

The authors declare no competing interests.

Additional information

Supplementary information The online version contains supplementary material available at <https://doi.org/10.1038/s43247-022-00530-6>.

Correspondence and requests for materials should be addressed to G.W.K. Moore.

Peer review information Communications Earth & Environment thanks David Babb and the other, anonymous, reviewer(s) for their contribution to the peer review of this work. Primary Handling Editors: Jan Lenaerts, Joe Aslin.

Reprints and permission information is available at <http://www.nature.com/reprints>

Publisher's note Springer Nature remains neutral with regard to jurisdictional claims in published maps and institutional affiliations.



Open Access This article is licensed under a Creative Commons Attribution 4.0 International License, which permits use, sharing, adaptation, distribution and reproduction in any medium or format, as long as you give appropriate credit to the original author(s) and the source, provide a link to the Creative Commons license, and indicate if changes were made. The images or other third party material in this article are included in the article's Creative Commons license, unless indicated otherwise in a credit line to the material. If material is not included in the article's Creative Commons license and your intended use is not permitted by statutory regulation or exceeds the permitted use, you will need to obtain permission directly from the copyright holder. To view a copy of this license, visit <http://creativecommons.org/licenses/by/4.0/>.

© The Author(s) 2022